RESULTS OF IMPACT ANALYSIS ON HST SERVICE MISSION 3B SOLAR ARRAYS

A.Moussi [1] [2] , G.Drolshagen [3] , J.A.M.McDonnell [4] , J.C. Mandeville [2] , A.Kearsley [5]

[1] CNES, 18 Av. E. Belin, 31400 Toulouse, France.
[2] ONERA/DESP, 2 Av. E. Belin, 31400 Toulouse, France, fax:33 5 62252569.
[3] ESA/ESTEC, Keplerlaan 1, NL-2200 AG Noordwijk, The Netherlands.
[4] PSSRI, The Open University, Milton Keynes, MK7 6AA, U.K.
[5] Dept of Mineralogy, The Natural History Museum, London, SW7 5BD, UK.

ABSTRACT

It is important that our knowledge of space debris flux and its potential growth is kept up to date for effective modelling. In one particular critical size regime, knowledge of the sub-mm particle population can only be gained by in-situ detectors or the analysis of materials exposed to space.
The solar arrays of Hubble Space Telescope provide a unique opportunity to gain data about these solid particles in the LEO environment and, significantly, evolution of the flux over the decade from 1993. The large area exposed for more than eight years provides high precision particle flux data up to the particle size range of 300 microns. With careful chemical analysis of residues it is also possible to distinguish between debris and meteoroids. Together with damage equations, it has been possible to identify flux distributions as a function of particle diameter.
Key aspects of the survey are described, and results of the impact analysis are presented for crater diameters ranging from 3 micrometers to 7 mm. The results are compared with those obtained after the first (1993) post-flight analysis, and with the models currently used to simulate the space environment.
In conclusion we find good support for the models and fair agreement between PFA1 and PFA2 at medium crater dimensions although, for particles smaller than 5 microns, there is a significant discrepancy.

1. INTRODUCTION

1.1. Solid Particle Detection

In order to achieve accuracy in debris and meteoroid flux modelling, information on the solid particle population is needed. However, ground-based measurements address only the largest objects (larger than 10 cm) so micron to mm sized particles have to be studied by in-situ detectors, either active sensors or simply returned space-flown surfaces.
During the last three decades, several dedicated surfaces designed to sample the low Earth orbit impact environment have been deployed in space (e.g. Long Duration Exposure Facility, Zolensky et al, 1995 or Orbital Debris Collector experiment on Mir, Hörz et al.,2000).
In addition to dedicated particle collectors, a wealth of information has been gained from retrieved spacecraft hardware such as the large solar arrays panels from the Hubble Space Telescope (Graham et al., 2001).

1.2. Passive Detection: Information gained

After exposure to the space environment, spacecraft surfaces are dotted with a large number of impact craters caused by meteoroids and debris. A first cumulative flux, as a function of the crater diameter, may be deduced from the number of impacts observed divided by the area x time product. The reliability of the flux estimation increases with the studied surface area and exposure time. From comparison of the size of the measured impact features and data from laboratory calibration experiments, the flux for solid particles can be determined as a function of particle size.
A further step, chemical analysis of projectile remnants, allows discrimination between meteoroids and debris.

2. HST POST-FLIGHT ANALYSIS

2.1. HST Mission

The present post-flight impact study, under an ESA contract follows a similar protocol to that undertaken after the first servicing mission in 1993 (PFA1) when only one wing was retrieved.
The two wings of solar arrays retrieved in March 2002 were placed in orbit in December 1993. The total exposure duration was 3,011 days or 8.24 years. The HST orbit was nearly circular at a mean altitude of 600 km and an inclination of 28.5°. A total of 40 m2 covered by solar cells provides the largest survey area of a single substrate ever retrieved. The area per time product is four times larger than that from the first post-flight analysis and has extended the measurements to the largest particle sizes ever recorded.
The solar array is divided into two wings, +V2 and –V2, each with an upper and a lower blanket, defined by their position on the central drum.
Each wing consists of 10 Solar Panel Assemblies (SPA), denoted by the letters A to E and AA to EE. The solar arrays are thin, with a total thickness of about 700 microns, and flexible. Each cell is protected by a cover glass and measures 40.2 by 20.8 mm. The construction of the cell is shown in Figure 1. Impact features on the cover glass are easily found on the front side of the cells, but detection is much more difficult on the resin-impregnated fibre-glass of the back side.

Because of the complex composition of the cell, particularly the coverglass, discrimination between components of substrate and impactor residue may be difficult.

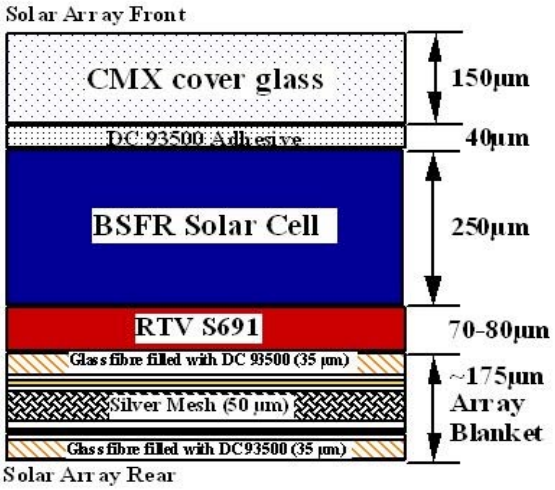

Fig. 1. Cross section of a solar array from HST.

2.2. Large Impacts Survey

The study began with two periods of investigation where panels were deployed in a clean room at ESTEC, in November 2002 and February 2003. Both faces of the wing -V2, and only the front face of wing +V2 were studied. In addition to a global visual survey, a systematic photographic scan was performed with a digital camera at low resolution (10 images per SPA) and medium resolution (29 images per SPA). A low-resolution survey of the entire front surface was also made with a Hirox video microscope; all craters larger than 3.6mm were recorded. On a smaller area, all craters larger than 2.4 mm were recorded, and a "catch all" survey was performed on 0.45m^2 of surface in order to record all craters larger than 100 micrometers, i.e. all impact features visible to the naked eye.

A co-ordinate system for each blanket was used to identify craters and map the impacts on the surface. This was also used on wing –V2 to match the pairs of impact features where the impact had damaged both faces. An example is shown in figures 2 and 3.

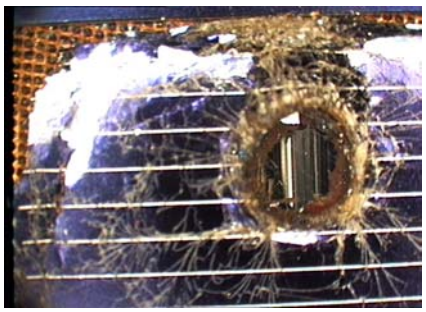

Fig.2. A large impact feature on the front face caused by an impact on the rear side (Figure3). The hole diameter is about 2.5mm.

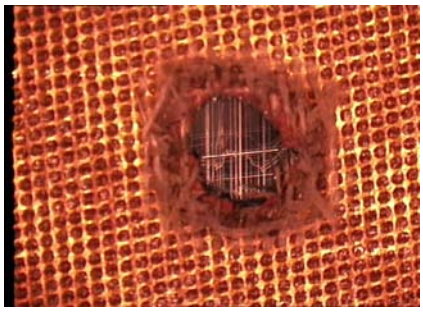

Fig.3. The large feature on the entry side (rear) corresponding to the damage on Fig.2. The hole diameter is about 2.5mm.

2.3. Detailed Survey in Laboratory

The global survey in a clean-room was followed by detailed surveys of smaller impacts on selected surfaces cut from SPA AA on wing –V2. An entire row, and randomly chosen solar cell samples were studied in the laboratories of the Office National d'Etudes et de Recherches Aerospatiales (ONERA) at Toulouse in France and at the Natural History Museum (NHM) in London, in the United Kingdom.

A high-resolution survey was performed with optical and scanning electron microscopes and was followed by the chemical analysis of projectile remnants in about 150 craters. The facilities used for this study were two JEOL 840 SEMs, and a JEOL 5900LV SEM, each fitted with an Oxford Instruments energy dispersive X-ray spectrometer.

The higher resolution provided by SEM enabled characterisation of all craters larger than 3 microns. Figure 4 gives two examples of craters of different sizes, observed with SEM. The mean density of impacts found was about 12 impacts larger than 3µm, per cell. For a direct comparison with the previous post-flight analysis, cells from the wing retrieved in 1993 were re-analysed with this new equipment.

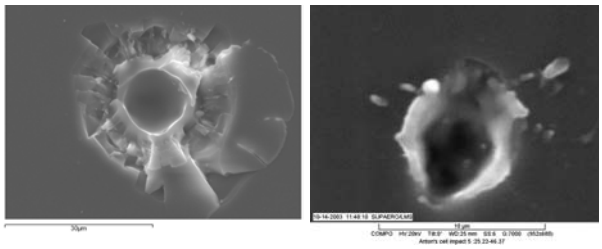

Fig.4. Two craters observed in secondary electron images, a prominent feature with a diameter of about 30µm (left) and a very small and oblique one (right, diameter about 3µm).

3. RESULTS

3.1. Impact Morphology

A simple classification system was devised during PFA1 to enable grouping of the most frequent impact morphologies [Carey et al., 1995].

The 4 main damage zones and their measured external diameter, are shown in figure 6. They are: the pit or hole (Dp); the shatter zone (Dsh); the conchoidal (Dco) or spallation zone (Dis or Dos) and the maximum damage zone (Dm). Within each zone, several criteria are used to classify the impact: the shape, colour, texture and distinguishing features like a halo or cracks.
There are four main classes of impacts:

- Front-Top (FT) impacts are features observed on the glass side caused by impacts onto the same face, They are subdivided into 4 types, from I to IV, as a function of the increasing projectile energy (examples are shown in the right column, figure 5)
- Front-back (FB) impacts are observed on the front side but caused by impact on the rear side. They are classified from pre-A to C. (figure 5, left column)
- Rear-Top and Rear-back (RT, RB) impacts are features observed on the fibre glass side caused respectively by impact on the front or on the rear face.

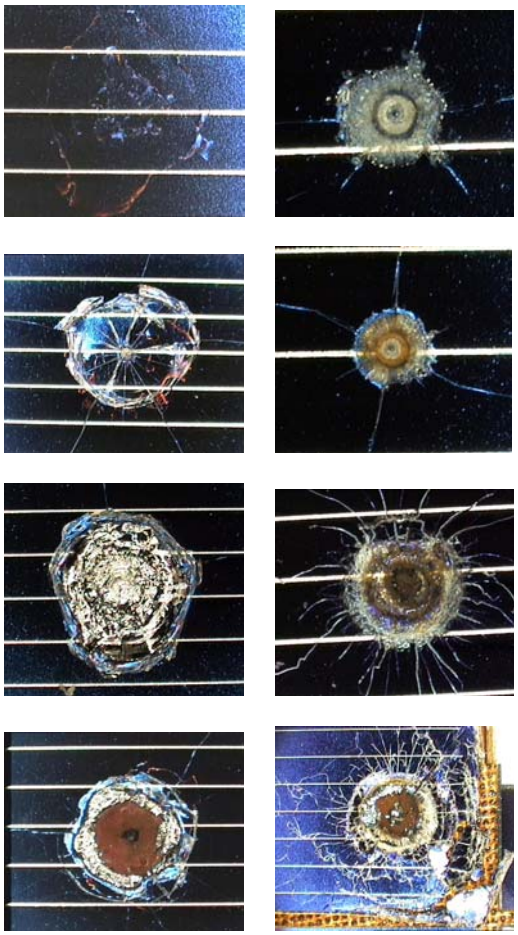

Fig.5. Impact features morphologies: types FB pre-A to perforation (left) and types FT II to perforation (right).

A database was created to include the following information for each impact feature: the location on the array; the material penetrated; the entry side; the type of impact (based upon the classification and measured morphological parameters). The total number of impact entries stored in this database is 1400, including data from all resolutions surveyed.

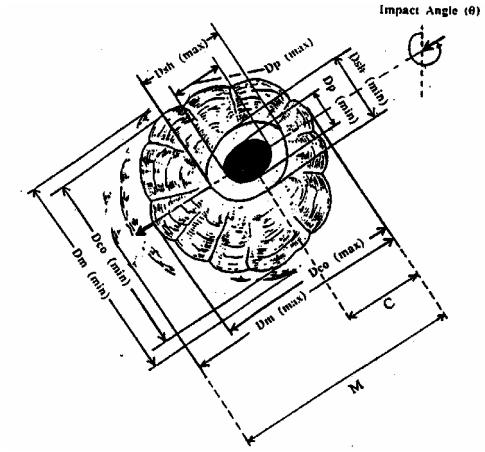

Fig.6. Measured parameters of impact craters on the solar cell surface. In case of an oblique impact, more parameters are measured (Carey et al.)

3.2. Crater Size Distribution

3.2.1. Most Significant Damage

Across the entire area of the sun-facing top of the wings, we found about 330 perforations, or large features close to complete perforation. Among them, only one third were caused by front impacts, the remainder being front-back features.
The largest impact measured had a conchoidal diameter of about 6mm, corresponding to a maximum damage zone of 20mm (a half cell destroyed). Only 3 front-back impacts were larger than 5mm, and none of front-top impacts. The most numerous substantial features of damage on the HST solar arrays were caused by rear-incidence impacts. This is due to impact beneath the complex multi-layer structure and the consequent broad outer spallation of the overlying coverglass. However, the largest FT craters were in the size range 4 to 5 mm and most of FB impacts had a diameter of 3 to 4 mm.
The total density of clear, full-thickness perforations on the entire array was about 4 holes per square metre and for most (90%), the corresponding feature on the opposite side was identified. The 150 pairs identified on –V2 wing provide a wealth of data on solar cell behaviour, very useful for improvement of the damage equations. The spatial distribution of the craters, for given limiting sizes, is not consistent with a uniform distribution, with more craters being observed on the inboard sides of the array.
In addition to the global survey, a set of 30 large impact features, both FB and FT, were analysed with a confocal microscope. This instrument produces 3D representations of the crater form and permits estimation of the volume of secondary material ejected into space by the impact. The volume of ejecta formed by an impact on the front surface of a cell is about 50 times that of the projectile. The volume of brittle material ejected from the cell front by a rear incidence impact is 100 to 300 times the volume of the projectile. This ratio shows the importance of the ejection process in the proliferation of micro-debris.

3.2.2. Fluxes in Crater Diameter

Figure 7 shows the cumulative flux of front incident impacts obtained from post-flight analysis 2 as a function of crater diameter. It combines the results from the different surveys and resolutions. Each component was simply obtained by dividing the number of impacts found during the survey by the scanned area and the exposure time to space. Then, each flux segment was stitched by projection to the neighbouring smaller size flux across the point where the imaging resolution had become inadequate for effective crater detection, and the flux appeared to 'roll-off' to a horizontal line. The resulting plot (figure 7) gives the cumulative front flux for crater sizes from 3 micrometers to 5mm. However, the sample numbers are insufficient for us to consider the largest size impact flux reliable. An even larger survey might have revealed rare impacts plotting to the right of the region where the curve approaches the vertical (i.e. apparent zero flux).
The plotted flux of figure 7. includes all solid particles irrespective of origin, both natural micrometeoroids and artificial debris. Chemical analysis of impact residue is necessary to discriminate between the two origins.

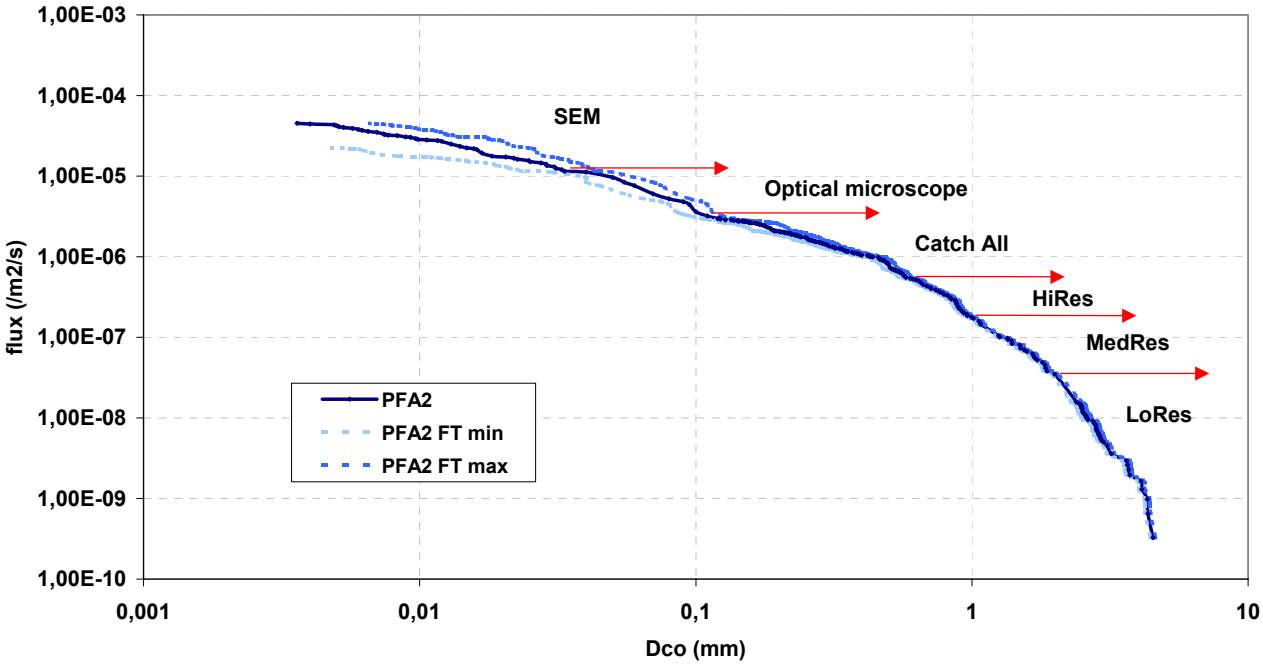

F

Fig.7. Cumulative flux on the front side (FT impacts only) of the HST solar cells as a function of conchoidal diameter with error margins due to measurement, upper (max) and lower (min) limits. The plot shows results from the different surveys (different resolutions) separated by arrows.

3.3. Residue Analysis

3.3.1. Protocol and Main Results

A complete residue analysis was done on 156 impacts located on 30 cells from SPA AA on –V2 wing. Using the facilities described in part 2.3, selected impacts with diameters from 4 to 2000 microns were analysed. The protocol used was the same in both laboratories. An initial scan was performed with SEM in secondary electron mode (SEI) to locate impacts, craters appearing as a dark central cavity surrounded by a bright ring. Then a second survey with back-scattered electron images (BEI) showed areas with differing composition, possibly indicating residue. The final step was X-ray spectrometry from selected areas complete elemental mapping of the crater when residue was not obvious. Small impacts (<100 µm) were mainly elongate features generated by oblique impact, and residue was usually found in the pit, at the end of the projectile trajectory, or on the melted lip.

By overlapping the complex spectrum of the background cover glass with that of the residue, it was possible to deduce the chemical signature of the projectile. This signature was compared with elemental enrichment assemblages representative of important debris or meteoroid components. The origin of the projectile was successfully determined for three quarters of the craters, a function of modern instrumentation, and with a good correlation between the results from the two laboratories.

3.3.2. Distribution MM/SD

Among the 156 impacts, 69 were identified as space debris impacts, 50 features resulted from impacts by meteoroids and 37 had unknown origin as diagnostic elemental assemblages were not found, or could not be interpreted. Most of meteoroids were silicate (50%) or phyllosilicate (10%) in composition, others were mainly sulphide. This natural particle distribution is very close to that observed during PFA1.

Space debris remnants were mainly aluminium-rich (45% aluminium debris and 45% of aluminium oxide), the rest were sodium-rich residue.
As figure 8 confirms, most small impact craters (<30 microns conchoidal diameter) were created by space debris. This size range is dominated by aluminium and aluminium oxide objects resulting from solid rocket motor (SRM) combustion dust.
However, meteoroids were shown to be responsible for the majority of impacts larger than 30 microns and the few largest craters (larger than 3 mm) were also more often caused by natural particles. This part of the study provided meteoroid and debris proportions for six main size ranges (0 to 20µm, 20 to 40µm, 40 to 60µm, 60 to 90µm, 90 to 1000µm, and larger than 1000µm). The relatively small number of undetermined features were allocated proportionately to probable micrometeoroid and space debris fluxes.

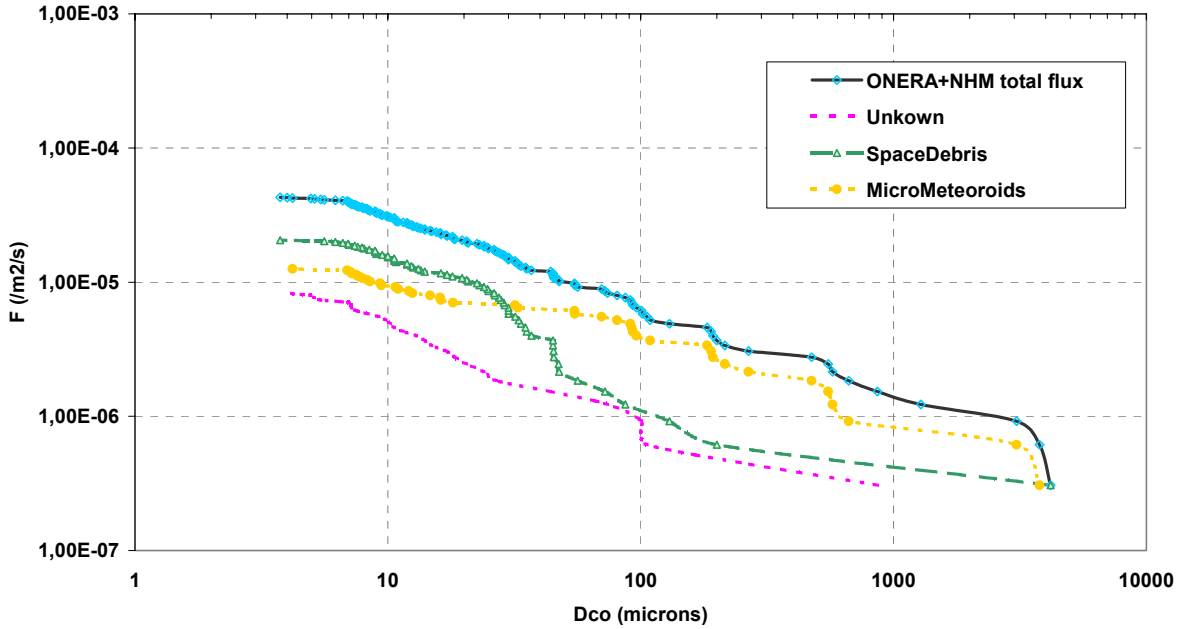

Fig.8. Residue analysis results: cumulative fluxes as a function of crater size. The dark continuous line is the total flux, the dashed line with small triangles represents the flux of space debris, the bright dotted line is the micrometeoroids flux and the dashed dark line is the flux of unknown origin particles.

3.4. Damage Equation and Flux Conversion

It is necessary to convert the cumulative feature size flux given in figure 7 to be able to compare it with models or other in-situ data. For this purpose, a set of empirical damage equations was specially derived for the Hubble and EuReCa solar panels (Drolshagen et al., 1997; Taylor et al., 1997).
For each kind of feature, velocity and density of the impactor are assumed (either those of a meteoroid or a debris) and a unique particle diameter can be derived from crater size.
The more reliable equation is for projectiles impacting the solar cells from the front direction, the most abundant features observed in this survey. However, no systematic work has yet been performed to assess the conditions for the semi-infinite/finite transition for complex solar cell substrates, as has been the case for aluminium and Teflon. Even if the regime where D_{co} approaches the particle diameter for largest features is taken into account, this effect still seems to be underestimated in the current damage equations. Further studies need to be performed to resolve this issue, and the steep 'drop-off' segment of the curve on figure 9 will probably rise to intercept the X-axis at a larger particle size when the underestimation of diameter from D_{co} is more properly accounted. Indeed, regarding the surveyed area of the array in the light of earlier surveys on other substrates, we might have expected the plot to extend to particle diameters of 500µm rather than 300µm.
The FB size calibration also needs to be improved because D_{os} (the outer spall diameter, replacing D_{co} as the entry parameter in the equation) has not been established as a reliable parameter. The crater diameter does not appear to vary systematically; a pre-A crater has about the same diameter as a perforation. Perhaps another criterion should be included in the damage equation, the ratio of pit or hole diameter to D_{os}. We now have a very useful set of data for this purpose, with measurement of paired features from the survey of the wings, coupled with laboratory calibrations.
The two other damage equations concern impact features on the rear surface, coming from the rear or results of impacts on the front. Unfortunately, it is very difficult to produce reliable calibration because, in the case of HST, the flexible composite backing hinders recognition of impacts and their measurement. The task is made even worse as the glass fibre weave is larger than, or equal to, the scale of most impacting particles.

For the rear surface impact features we have no conchoidal spall, and D_{co} is replaced by Dl (the crater lip diameter) or D_{sc} when a scorched zone exists around the central pit. Using these four damage equations, fluxes relative to the four types of features were derived. The density assumed for space debris is 4g/cm^3 with a mean velocity of 10km/s, and the density assumed for meteoroids is 2.5 g/cm^3, with a velocity of 21.4km/s, as was used for PFA1.

4. DISCUSSION

4.1. Flux in Particle Diameter

The most interesting flux is that for particles from the sun direction, causing front-top features.
To obtain the final flux as a function of particle diameter, we firstly derived two fluxes from the one in figure 7 with two sets of appropriate assumptions on density and velocity corresponding to the two limit scenarios. In the first, all impactors are assumed to be space debris and in the second one, all projectiles were meteoroids. The final consolidated flux (shown on figure 9) was obtained by combining the two fluxes with sizes apportioned according to the proportion of meteoroids and debris in each size range determined by the residue analysis.

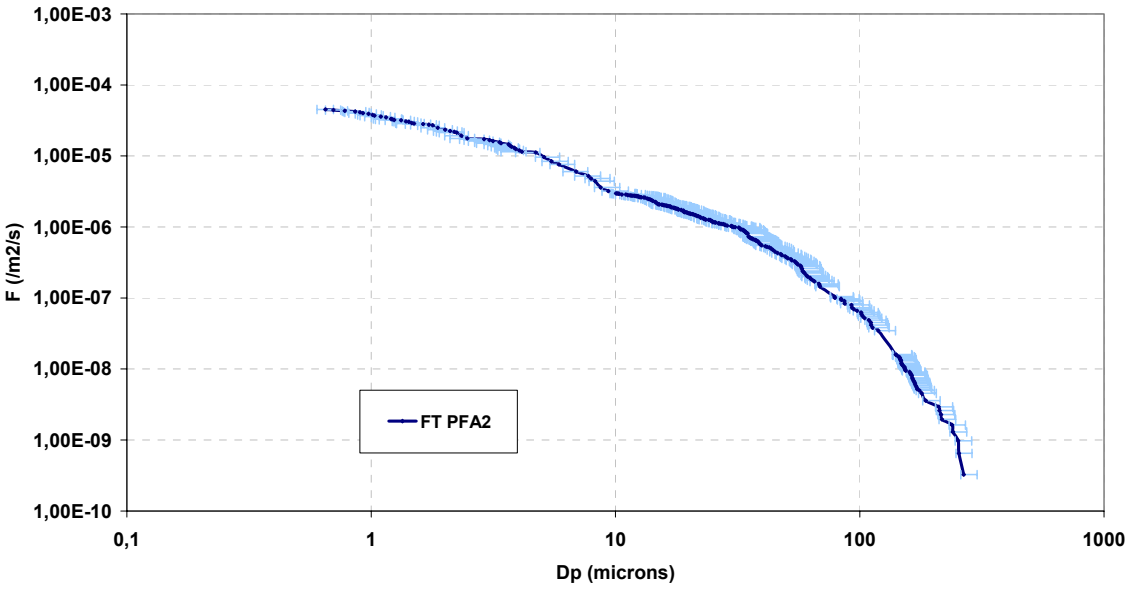

Fig.9. Cumulative flux (front side of the HST solar arrays) as a function of the particle diameter Dp after conversion.

4.2. Comparisons

4.2.1. Comparison with HST PFA1

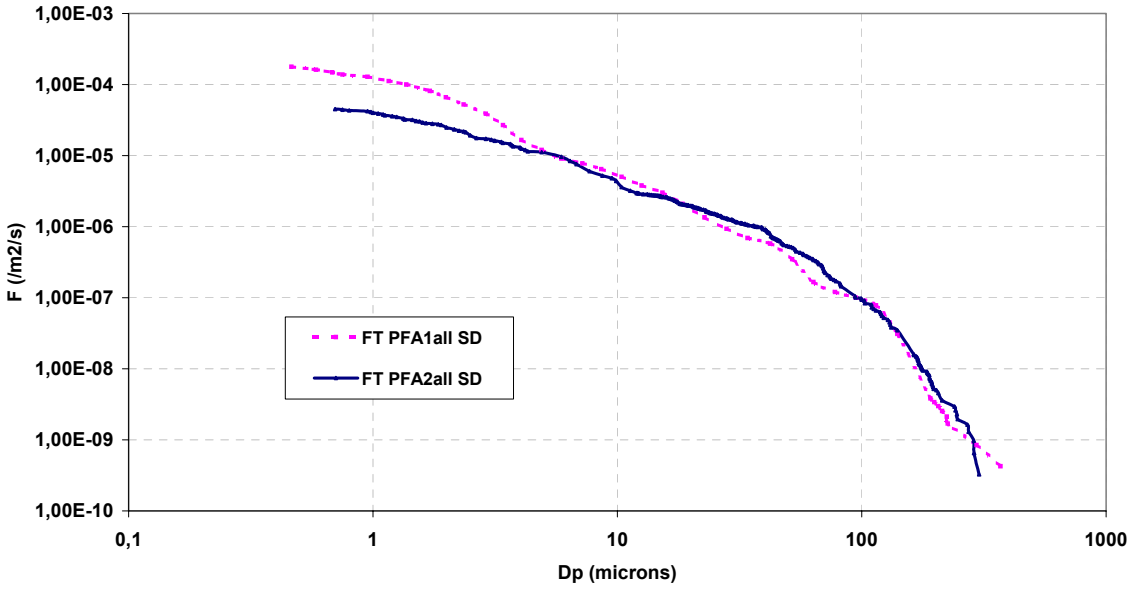

Fig.10. Cumulative flux after post-flight analysis 2 (dark continuous line) compared with cumulative flux of PFA1 (dashed line). Fluxes are functions of particle diameter and both data sets have been converted the same assumptions.

Figure 10 is a comparison of PFA2 front flux with the flux obtained during the impact survey of the first HST array retrieved in 1993 (Carey et al., 1995). To be valid, this comparison requires that the fluxes be derived with the same method and assumption. Figure 10 presents comparable fluxes derived with the same assumptions for density and velocity of space debris.
Statistical error as a result of a relatively low sample number may be significant for the largest craters, while fluxes for the smallest crater sizes may be systematically too low, due to overlooked craters in the 'tail-off' recorded by each survey method. The difficulty of determining mean diameter for irregular features could also be an additional source of error.
The new measured crater fluxes are in good agreement with the previous one, although they do appear somewhat lower than in 1993 at crater sizes below 5 μm. To further investigate this discrepancy, 16 cells from the 1993 post-flight analysis and 18 from 2002 were studied at ONERA, using exactly the same protocol. Resulting fluxes were similar to those we had previously determined, and confirming the decrease of very small objects between 1993 and 2002. However, the number of impacts per cell varies widely (from 7 to 22), so it is possible to derive very different small crater fluxes if only a few cells are examined. In order to minimise this problem of poor statistical sampling or spatially-associated swarms of secondary impacts, we selected samples from a long transect across the array. It is now unlikely that the reduction in small craters is an artefact. However the main contribution to the small particles debris family is the exhaust of Al_2O_3 'slag' particles and dust during operation of solid rocket motors for orbit transfer manœuvres. The orbital lifetime of micron-sized particles does not exceed a few days at the inclination of HST and the use of solid rocket motor has declined since the launch of Hubble (see Figure 11).

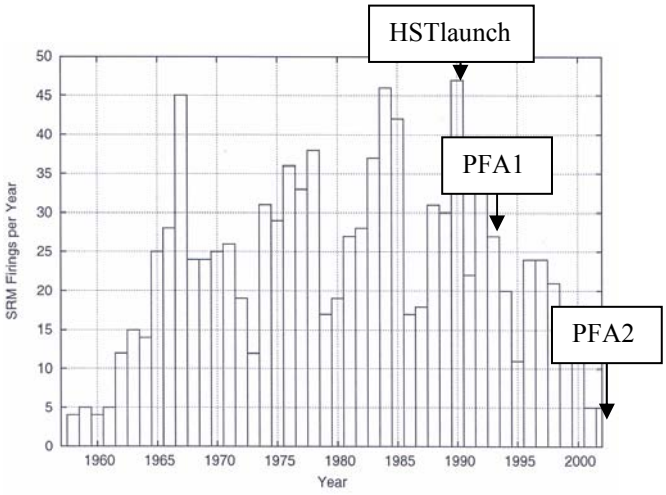

Fig.11. Solid Rocket motor firings per year since 1959.

As a conclusion, it is perhaps not surprising that we found less small debris than during the first post-flight analysis, which may have sampled the peak of solid rocket motor firing in 1990.
Front-back fluxes for 100 micron particles are the same for PFA1 and 2. (about 3.10^{-8} impacts per m^2 per second) and similar to the rear top flux ($2.10^{-8}/m^2/s$), to be expected as Front Back features are the front face of large Rear Top impacts. However, in contrast to the decrease in very small objects, in figure 10 we see a small increase in flux between 30 and 100μm. Front Back, Rear Top and Rear Back fluxes each show a similar increase for particles larger than 30μm.
We suggest that further study is needed on effects of variation in solar activity during the two exposure periods of HST panels. The mean atmospheric density varied widely between 1990 and 2002, and might make substantial changes in the lifespan of orbiting particles.

4.2.2. Comparison with Models

Several models are currently used to assess the meteoroid and debris environment, mainly based on in-situ and ground based observations. The most famous model for the meteoroid population is the Grün model, and three widely used models for space debris are ORDEM96, ORDEM2000 and MASTER2001, but ORDEM 2000 gives a little higher flux than the two others. So in the figure 12, only results from ORDEM96 and MASTER2001 (each coupled with Grün) are compared with PFA2 flux. The MASTER (Meteoroid and Space Debris Terrestrial Environment Reference Model) is based on semi-deterministic analysis and prediction techniques, supported by data from a number of fragmentation experiments and compilation of the current debris sources. ORDEM (Orbital Debris Environment Model) uses empirical estimates of the orbit populations from ground-based observations and surfaces returned from LDEF. It is valid for particle diameters down to 10 μm and approximates the orbital debris environment for a limited number of representative orbits.
Estimated fluxes were calculated for a randomly tumbling plate. Figure 12 shows good agreement with the predicted fluxes at small (<5μm) and intermediate sizes (30 to 200μm), but an overestimation for particles sizes in the range 5-30 microns. Beyond 200μm particle size, models seem to overestimate the flux but this is mainly due to the detection limit of HST arrays combined with an underestimation of diameters in damage equations for large craters.

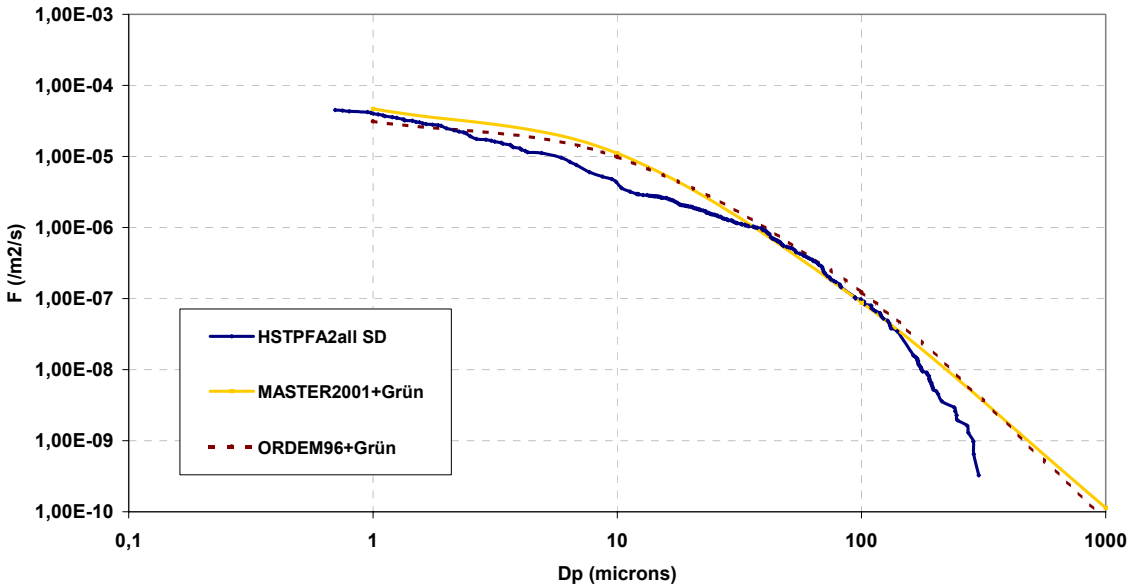

Fig.12. Cumulative front flux for HST arrays PFA2 compared with flux predicted by two models: MASTER2001 for debris coupled with Grün flux for meteoroids (bright line) and ORDEM96 with Grün (dashed line).

5. CONCLUSION

Post-flight visual and microscopic examination of the solar arrays of the 2002 HST service mission has permitted analysis of impact damage from micron to near centimetre scale. As with the first array study following 1993 recovery, chemical analysis by electron beam techniques has been used to determine the nature and origin of the impactors. Improvements in instrumentation have led to greater success in discrimination between space debris and meteoroids. In very small craters, aluminium oxide space debris from solid propellant apogee boost motors dominates. In the medium size range, meteoroids dominate but space debris is still a significant factor. Flux distributions have been determined for both exposed faces as a function of crater diameter, and damage equations relating crater characteristics to projectile parameters have been applied. Data have been compared to the ESA MASTER and NASA ORDEM models, with good agreement, and to the results from the first post-flight analysis. The most obvious change is a reduction in very small particles, related to decrease of solid fuel booster operation after a peak near 1993.

6. ACKNOWLEDGEMENTS

This work was done under the ESA/ESTEC Contract 16283/NL/LvH 'Post-Flight Analysis of HST Solar Arrays – 2002 Retrieval'. All contributions from the study team members to the described results are gratefully acknowledged.

7. REFERENCES

Carey, W.C., Fowler, M., Griffiths, A.D., et al. Hubble Space Telescope Micrometeoroid and Debris Post Flight Analysis. In: Carey, W.C. (Ed.), Space Applications Services (SAS), Technical and Final Report, ESA contract 10830/94/NL/JG, Sept. 1995.

Drolshagen, G., McDonnell, J.A.M., Stevenson, T.J., et al. HST solar array impact survey: Revised damage laws and residue analysis. Adv. Space Res. 19, 239-251, 1997.

Graham, G.A., Kearsley, A.T., Drolshagen, G., et al. Microparticles impacts upon HST solar cells. Adv. Space Res. 28, 1341-1346, 2001.

Graham, G.A., McBride, N., Kearsley, A.T., et al. The Chemistry of micrometeoroid and space debris remnants captured on Hubble Space Telescope solar cells. Intern. Journ. of Impact Engineering 26, 263-274, 2001.

Grün, E., Zook, H.A., Fechtig, H., et al. Collisional balance of the meteoritic complex. Icarus 62, 244-277, 1985.

Hörz, F., Zolensky, M.E., Bernhard, R.P., et al. Impact features and projectile residue in aerogel exposed on MIR. Icarus 147, 559-579, 2000.

Kearsley, A., Drolshagen, G., McDonnell, J.A.M., et al. Impacts on Hubble Space Telescope solar arrays: discrimination between natural and man-made particles. submitted to Adv. Space Res. Sep 2004.

McDonnell, J.A.M., Griffiths, A.D., Herbert, M.K., et al. Meteoroid and debris flux and ejecta models. In: McDonnell, J.A.M. and Griffiths, A.D. (Eds.), UniSpace Kent (USK), Final Report, ESA contract 11887/96/NL/JG, December 1998.

Taylor, E.A., Kay, L., Shrine, N.R.G. Hypervelocity impact on semi-infinite brittle materials: fracture morphology related to projectile diameter. Adv. Space Res. 20, 1437-1440, 1997.

Zolensky, M.E., See, T.H., Bernhard, R.P., et al. Final activities and results of the long duration exposure facility meteoroid and debris special investigation group. Adv. Space Res. 16, 53-65, 1995.